From Aluminum Dissolution in Supercapacitors to Electroplating: A New Way for Al Thin Film Deposition?

ADVANCED MATERIALS INTERFACES
Open Access
www.advmatinterfaces.de

From Aluminum Dissolution in Supercapacitors to Electroplating: A New Way for Al Thin Film Deposition?

Pietro Zaccagnini, Lars Henning Heß, Luisa Baudino, Marco Laurenti, Mara Serrapede, Andrea Lamberti, and Andrea Balducci*

The present work addresses a new finding observed while performing aluminum dissolution experiments for supercapacitors (SCs) stability investigation. Supercapacitor (SC) electrodes based on carbon-coated aluminum foils are electrochemically cycled in harsh conditions into bis-trifluoromethylsulfonyl imide (TFSI)-based electrolyte and using Acetonitrile (ACN) as solvent. Dissolution of aluminum is observed with subsequent plating on the carbonaceous surface of counter electrodes. Moreover, the same process can be reproduced also on standard SC activated carbon electrodes. This mechanism can open the way to an effective strategy to achieve Al film deposition by electroplating becoming competitive with the most common copper counterpart.

1. Introduction

Supercapacitors represent one of the most promising electrochemical energy storage device complementary to rechargeable batteries.[1,2] The state-of-the-art technology relies on largely available and relatively cheap active materials and electrolytes, i.e., activated carbons and inorganic salts such as tetraethylammonium tetrafluoroborate ($TEABF_4$), dissolved into organic solvents, typically acetonitrile (ACN). These combinations warrant operating power greater than 10 kW kg^{-1}. However, the practical voltage window that can be exploited is limited to ≈3 V, above which several degradation phenomena on the electrode or in the electrolyte can occur.[3–6]

Several alternative electrolyte components have been proposed in the past years with the aim to increase the operating voltage, and thus the energy density of EDLCs.[6] At this point, it is important to remark that the electrochemical performance of EDLC is also strongly affected by processes occurring at the current collectors used in such devices, which are made of aluminum.[7] For this reason, while developing novel electrolytes, their interplay with the current collector needs to be carefully considered.

Among the proposed alternative salts, those based on the imide anions, i.e., bis-trifluoromethylsulfonyl imide (TFSI), are regarded with great interest due to their high chemical and thermal stability.[8–10] However, the main drawback associated to the use of these salts in electrolyte formulations is the occurrence of anodic dissolution at the aluminum current collectors. As reported in several studies, the aluminum substrate dissolves as Al^{3+} ions when subjected to high oxidation potentials. The dissolved aluminum ions react with the electrolyte mixture to form aluminum salts, the nature of which depends on the salt and solvents in the electrolyte system. While electrolytes containing BF^{4-} or PF^{6-} display the ability to prevent this dissolution process, those containing $TFSI^-$ are forming complexes which are typically highly soluble in organic solvent. Therefore, a strong anodic dissolution of the Al current collector is taking place when they are used. In the last years several studies have addressed this aspect, and it has been shown that the selection of solvents displaying low dielectric constant, i.e., 3-cyanopropionic acid methyl ester (CPAME), and the use of highly concentrated solution are interesting strategies to minimize the Al dissolution and guarantee the realization of high voltage EDLCs with high cycling stability.[11–19]

It is interesting to observe that the dissolution of Al, although deleterious for the stability of EDLCs, is a process of great interest because it could be used for the electrodeposition of this metal. Currently, Al is plated using baths consisting of low melting point aluminum halides such as $AlCl_3$ or $AlBr_3$, either mixed with some metal hydrates or in non-polar solvents.[20–23] Aluminum halides are toxic and expensive, as well as highly poisonous if dispersed in the environment. Furthermore, they are flammable and corrosive. This makes them an appealing solution for technological purposes, however, from a sustainability point of view, bath

P. Zaccagnini, L. Baudino, M. Laurenti, M. Serrapede, A. Lamberti
Department of Applied Science and Technologies – Polytechnic of Turin
Corso Duca degli Abruzzi 24, Turin 10129, Italy
E-mail: pietro.zaccagnini@polito.it
P. Zaccagnini, A. Lamberti
Centre for Sustainable and Future Technologies – Italian Institute of Technologies
Via Livorno 60, Turin 10144, Italy
L. H. Heß, A. Balducci
Institute for Technical Chemistry and Environmental Chemistry and Centre for Energy and Environmental Chemistry Jena (CEEC Jena) – Friedrich Schiller Universität
Philosophenweg 7a, 07743 Jena, Germany

The ORCID identification number(s) for the author(s) of this article can be found under https://doi.org/10.1002/admi.202202470

DOI: 10.1002/admi.202202470

solutions based on these salts are not environmentally friendly. A similar, but solvent-free system, was studied in 1928 when Keyes et al. performed plating on copper in a hot bath composed by Et_4N Br and $AlBr_3$. Briefly, the anode was Al, the electrodes were placed 1 cm apart, the current was 0.2 A cm^{-2} and the voltage was 16 V. The bath temperature was 100 °C. Although these processes are industrially established, their replacement with more convenient processes is nowadays regarded with high interest.

Among the possible alternatives, electrodeposition of Al is considered one of the most interesting. Aluminum was employed at first in integrated circuit technologies (ICTs) as metal for interconnects, and later substituted by copper during their scaling up. However, it can still be used to probe ICTs externally because of its higher endurance in corrosive environments, due to the presence of its native oxide. Indeed, Al has been exploited as a protective layer against corrosion since it can be further oxidized thanks to electrochemical processes like the "Eloxal" one.[24,25] Unlocking Al deposition from electrolytic environments without any halogenated precursors would allow for more efficient processes. Indeed, compared to physical and chemical vapor deposition techniques, electrodeposition offers higher deposition rates since it does not need to be performed in a vacuum. Further, it allows for thick films (up to 1 mm) deposition and ultra-pure (99.9%) phases deposition. Up to date, Al plating solutions prices are above 9 \$ L^{-1}. However, the best performing ones cost more than 25 \$ L^{-1}. These prices are calculated for 100 L of plating solutions containing organic salts and halogenated aluminum molten salts.[26]

In this work, we consider for the first time the electrodeposition of Al on carbonaceous substrates from highly concentrated organic electrolytes containing TFSI anion. The proposed electrolytic solutions benefit from the absence of halogenated aluminum salts making them less moisture sensitive and less prone to develop harmful gases such as HCl fumes. The proposed electrolytes rely on acetonitrile that is still flammable as other solvents proposed in recent literature, but still, the bath does not produce harmful gases.[27] The investigated electrolyte possesses the requirements for electrodeposition baths, and this electrodeposition process opens the possibility of exploration of novel, safe, and stable plating solutions for Al. It is shown how a one solvent and one salt electrolyte can be exploited to get Al plating, with the potential development of a low-cost bath solution.

2. Results and Discussion

With the aim to investigate the dynamics of the anodic dissolution of Al, we initially considered the electrolyte 1 M Et_4N TFSI in ACN. This electrolyte displays interesting transport properties, but it does not display the ability to prevent the anodic dissolution of Al current collectors.[28] We carried out an experiment in a three electrodes cell containing bare Al as working electrode (WE), an activated carbon electrode as counter electrode (CE) and a silver wire as quasi-reference electrode. Initially, we carried out a LSV from open circuit potential to 1.7 V versus Ag. During this experiment, which can be considered a bare Al dissolution experiment, an enormous change in current density was detected over the time of the experiment. The results and experiment description are reported in **Figure 1**. As shown in Figure 1a, after the dissolution potential of 1.1 V versus Ag, the current density produced at the working electrode (WE) raises from units of μA cm^{-2} up to tens of mA cm^{-2}. This point delimits the process stages 1 and 2 described in Figure 1e. When the potential was reaching 1.7 V versus Ag, a constant floating period of 12 h at this polarization condition was sustaining the dissolution phenomenon . During this stage of the experiment most of the charge contribution to the overall current density could not be properly buffered at the carbon-based counter electrode (CE) causing the CE to be polarized toward the instrumental limits as depicted in Figure 1b. The behavior of the not optimized CE was hence limiting the whole experiment because of hardware interruptions. The current evolution was so rough and intense (Figure 1c), that the CE could not properly equilibrate at the cathodic electrolysis limit due to the cation ($Et4N^+$) decomposition. In fact, the cathodic limit in this system is expected to be ≈−1.5 V versus Ag (or slightly below) as suggested by the CV and LSV profiles reported in refs.[28,29]. By increasing the weight, thus the capacitance, of the carbonaceous CE it was possible to properly buffer the whole charge coming from the complete dissolution of the Al WE. This caused an increase in the charging time of the CE and allowed the system to slowly reach a new (quasi) "steady state" at the CE which was, in our belief, the electrodeposition of Al. Indeed, in the whole time of the experiment enough dissolved Al^{3+} could have diffused at the CE whose potential energy got suitable for its plating. This non-spontaneous "rocking-chair", stripping-plating, mechanism is depicted in Figure 1e. Stage 1 belongs to the LSV period until the dissolution potential is reached. The current increases in a capacitive fashion and the counter electrode gets charged, indeed. In stage 2, dissolution is ongoing and Al cations are mainly diffusing in the bulk electrolyte because of the concentration gradient. By considering the areal capacities, reported in Figure 1d, the Al sample in the experiments had an average weight of 5.3 mg cm^{-2}, corresponding to a limiting dissolved capacity of Q_{Al} = 15.871 mAh cm^{-2}, addressed as Aluminum in Figure 1d. During stage 2, the charge produced by the Al sample, Q_2 = 7.153 mAh cm^{-2}, charges the counter electrode (and it can be properly screened). As the counter electrode reaches the right potential energy, in stage 3, also Al^{3+} reaches the CE interface and starts plating as suggested by the constant CE potential. During this stage, a Q_3 = 3.920 mAh cm^{-2} charge density is flowing. As the current density falls below 100 μA cm^{-2}, also the potential decreases in modulus as electrons might not be provided at a sufficient rate to keep the reaction going in the above mentioned conditions. The overall capacity of the dissolution period starting from stage 2 and considered to end at the instant as reported in Figure 1c was Q_D = 11.167 mAh cm^{-2}, referred as *Dissolution* in Figure 1d. These considerations on the capacities relate to a best-case scenario in which the stripping and plating processes both have full efficiency. In such cases, a 70.4 % of Al was dissolved in the dissolution period while only the 24.7 % was plated at constant potential. This process was repeated several times and can be considered reproducible. Further, at the end of all dissolution experiments, the Al sample was not fully dissolved, but rather it was in a powder-like state. This justifies the amount of computed Q_D lower than Q_{Al}.

To further investigate the deposition process, symmetrical cells containing two AC-based electrodes coated on Al current collectors were assembled and tested. At the anode side, the active material coating was providing a physical barrier to the

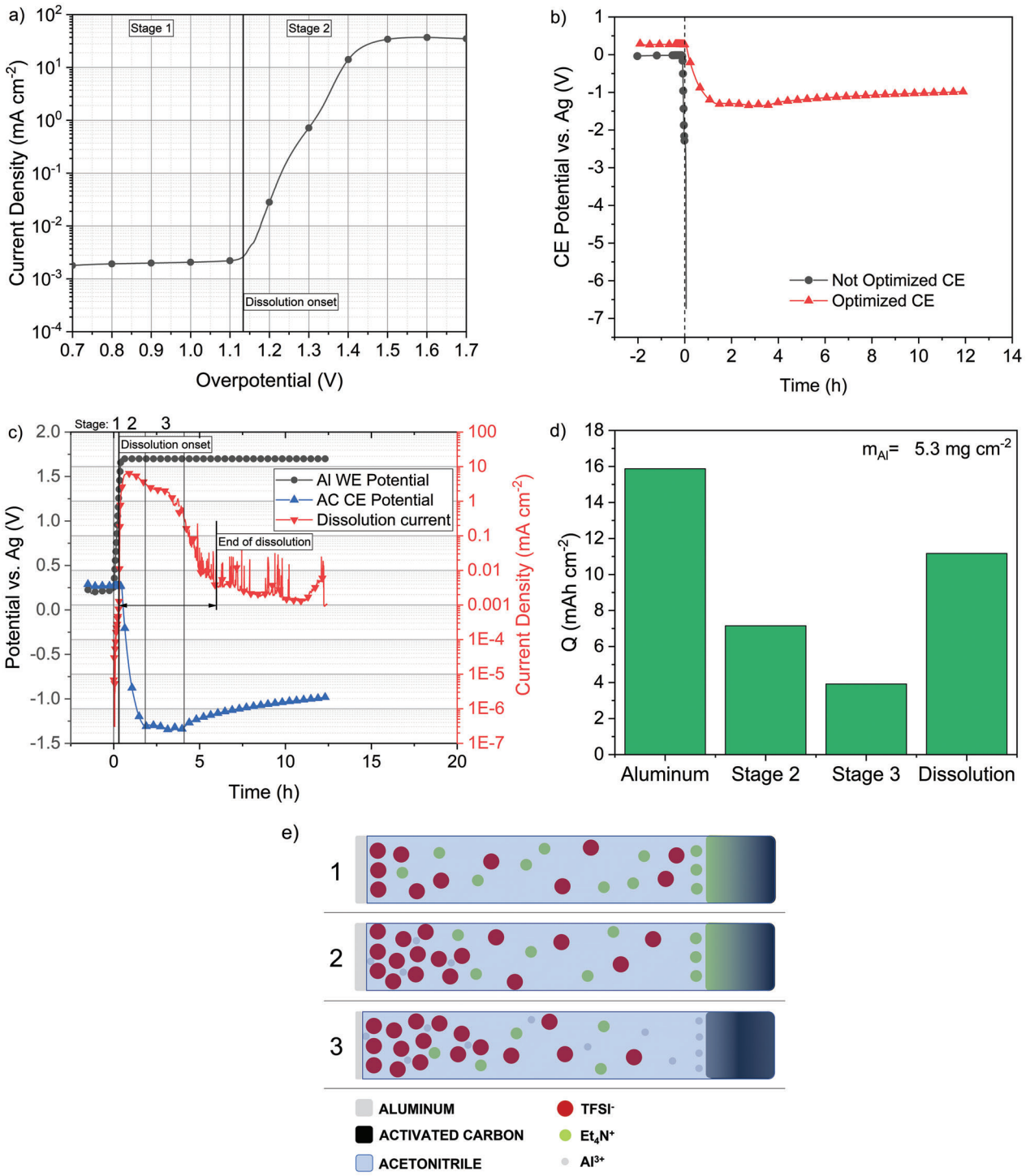

Figure 1. Al dissolution experiments with WE are consisting of bare aluminum and electrolyte 1 M Et_4N TFSI in ACN: in a) the LSV experiment showing the onset of bare Al dissolution, in b) the evolution of the CE in the case of not optimized and optimized CE. c) A complete dissolution experiment out of which charges were computed and reported in panel (d). e) The three process stages are schemed and highlighted.

dissolution process. As in the case of the solid electrolyte interface (SEI) in batteries, a physical barrier on the plated/stripped metal allows for uniform and rate controlled metallurgical processes.[30–32] This concept is also schematically depicted in Figure S1 (Supporting Information) and visibly observable as in the pictures of Figure S2 (Supporting Information). At the cathodic side, instead, the carbon material was exploited as plating substrate. The same tests were run in similar electrolytic conditions to get visible evidence of the deposition process. An electrochemical cell with copper as the WE, aluminum as the CE and

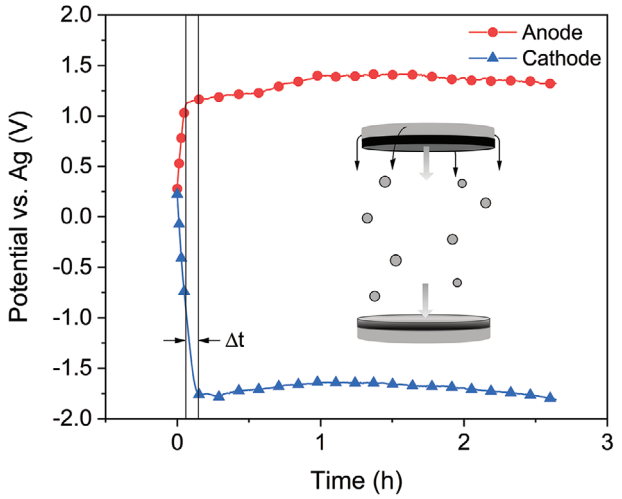

Figure 2. Al dissolution experiment with anode and cathode consisting of activated carbon electrode in 1 N $Al(TFSI)_3$ in ACN. The current density was 0.5 mA g^{-1}.

silver as the pseudo-REF was assembled to try the deposition procedure on a different substrate. The electrolyte was changed to 1N $Al(TFSI)_3$ in ACN to remove those cations which were not Al^{3+}. An opaque, light gray aluminum layer was observed to be deposited on the copper surface. Details concerning this exemplary result are reported in Figure S3 (Supporting Information). Moreover, a similar procedure was carried out in a 5 mL beaker cell to demonstrate Al electroplating on stainless steel in a batch solution. In detail, a 304 steel sample of 15 mm diameter was passivated by means of Kapton tape to expose just 8 mm in diameter of steel surface to the plating solution. An Al counter electrode was patterned to expose a 4 mm diameter surface to the electrolytic solution. The asymmetry between the two surfaces allowed to assure Al anodic dissolution at the counter electrode upon constant current plating. The galvanostatic plating was carried out at 2 mA cm^{-2}. Anode and cathode were 3 mm apart. Results of this experiment are reported in Figure S4 (Supporting Information). Optical images and EDS mappings highlight the presence of an Al deposit.

Further experiments were carried on with the electrolyte 1 N $Al(TFSI)_3$ in ACN to verify the plating process and excluding eventual contributions coming from the ammonium cations. The conductivity and the viscosity of the electrolyte are reported in Figure S5 (Supporting Information). The results are in line with the requirements for plating baths.[33] During the experiment a current density of 0.5 A g^{-1} was applied. The results of these experiments are depicted in **Figure 2**.

It can be observed that the cathode potential starts settling at a constant potential of ≈−1.6 V versus Ag, while the anode settles at the dissolution potential observed during the LSV experiments. This behavior was observed in several cells and can therefore be considered reproducible. Moreover, the carbon electrode masses were similar, and only a slight time delay, Δt, can be observed in the two electrodes. This is due to the different electrode specific capacitance with respect to anodic and cathodic polarizations which is usually different in organic electrolytes at anode and cathodes. We observed that after ≈2 h of plating the cathode potential was drifting as the deposition process was self-limited. Moreover, the fiber glass was always found to be preferably adhered to the deposited electrode only, and not on the dissolved one. For all the cells, a reduction in mass was observed at the anode, and an increase in mass at the cathode. Both anodes and cathodes were characterized from the physical chemical standpoint, to prove the Al plating process at the cathodes.

After the deposition process was completed, the deposited electrode was investigated by TGA and DTA. The same techniques were exploited to properly decompose and volatize all the electrolyte residuals from all anodes and cathodes. The same electrodes were analyzed under a Scanning Electron Microscopy (SEM) equipped with an EDS detector to evaluate the surface chemical composition. Finally, XPS measurements were performed to verify the actual aluminum deposition.

The results of simultaneous thermal analyses are shown in **Figure 3**. These measurements showed that more aluminum, prone to melt during the temperature ramp at ≈650 °C, was deposited on the negative electrode than on the positive one (see Figure 3a). It is also interesting to observe that the negative electrode consumes more thermal energy to melt the deposited aluminum compared to the positive one. This is well visible in Figure 3b, in which the peak intensity at 650 °C during the DTA analysis is more intense in the cathode sample with respect to the anode sample since there is more aluminum to be melted. The relatively lower peak of the anode sample can be due to the excess aluminum on the electrode coming from the decomposition of the electrolyte materials. The DTA analysis of the bare electrode sample shows a negligible peak at 650 °C since the heat capacity of the bulky current collector does not produce substantial heat absorption. Hence, for the other two samples, the amplified heat flow peaks at 650 °C (in the neighboring of the aluminum melting point) are most likely generated by small aluminum features on the carbonaceous active material phase. The result is confirmed by the work of Sun and Simon showing the effects of the melting behavior of aluminum nanoparticles.[34]

Electron microscope analyses were carried out on the same samples before and after heating to 700 °C to evaluate the composition of the electrodes' surfaces. The results are reported in **Figure 4**, where the same color code was used in all four images to represent the chemical composition. The EDS signals reported in the survey are the ones reported in **Table 1**, where the corresponding atomic percentages are provided. It is possible to appreciate that before the thermal test the two electrodes showed a surface composed mainly of sulfur, although fluorine ions were more abundant since they occur six times in the molecular structure of the salt. However, on the cathode sides, some relevant spots with greater aluminum concentration were present. This non uniform deposition behavior can be ascribed to not properly uniform current distributions over the electrode surface that might be caused by the T-Cell setup. Indeed, the stainless-steel connector possesses a smaller section (6 mm in diameter) with respect to the tested electrodes (12 mm in diameter). This causes an injection point of charges localized in a crown section in the middle of the circular electrode undertest.

It is worth noticing that these results come from the same measurement carried out on portions of the same electrodes after the thermal test. Since EDS signals come mainly from the surface, the aluminum traces on the cathode come from the

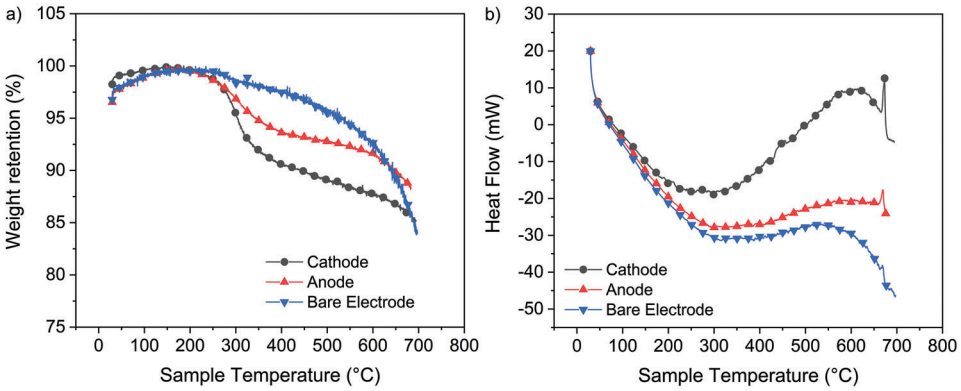

Figure 3. a) TGA showing that positive and negative electrodes show some weight loss after 600 °C with respect to a bare electrode caused by electrolyte residuals decomposition. b) DTA recorded during the TGA experiments showed a pronounced endothermal peak after 650 °C as expected because of the Al melting temperature.

plating process resulting in a decorated surface. Moreover, according to the elemental percentages reported in Table 1, while the salt stoichiometry is respected at the anode, this is not the case at the cathode, where especially the aluminum percentage is larger. The possible explanation concerning this result is that the Al^{3+} excess in solution caused by the dissolution phenomena could electrodeposit itself on the carbon surface so that the overall electroneutrality is preserved.

Specific surface area (SSA) measurements were carried out to study whether the electrodeposition process proceeds preferentially in the micropore volumes or in the mesoporous ones. The isotherms are reported in Figure S6 (Supporting Information). This result proves that the electrodeposition procedure does not produce any feature altering the isotherm shape, but it only reduces the SSA. The main results obtained from the SSA analysis are reported in **Table 2**.

All the quantities were computed by only taking into account the active material instead of also considering the additional weight of the deposited aluminum. It is worth noting that the BET surface area of the active material prior to the electrodeposition procedure is lower than the one of the YP-50F AC alone, which is 1666 $m^2\ g^{-1}$ according to the datasheet. This result is due to the account of low surface area weight provided by CB and Na-CMC. After the electrodeposition procedure, the BET surface

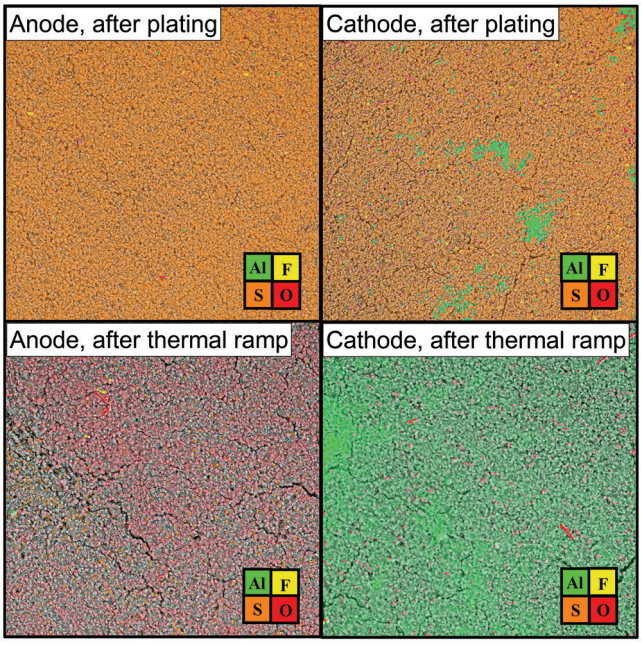

Figure 4. EDS mapping of the surface of the electrodes before and after the thermal analyses on both anodes and cathodes. Color intensities were not modified during the measurement. Refer to Table 1 for the abundance percentages.

Table 1. Atomic concentration percentages from EDS surveys performed on the electrode samples whose mappings are reported in Figure 4. According to the electrolyte stoichiometry: Al:S = 1:6 and S:F = 1:3.

Electrode	Element	Before	After
Anode	O	42.76	78.03
	F	35.89	7.85
	Al	**2.27**	**11.61**
	S	19.07	2.51
Cathode	O	42.56	65.44
	F	31.64	3.27
	Al	**10.72**	**29.52**
	S	15.09	1.76

Table 2. Specific surface area measurements results.

	Pre Al dep.	Post Al dep.
BET surface area [$m^2\ g^{-1}$]	1562.4	1025.7
Single point adsorption total pore volume of pores less than 40 nm at p/p0 = 0,9500 [$cm^3\ g^{-1}$]	0.715	0.475
t-plot micropore area [$m^2\ g^{-1}$]	1174.87	736.69
t-plot external Surface Area [$m^2\ g^{-1}$]	387.53	288.63
t-plot micropore volume [$cm^3\ g^{-1}$]	0.474	0.294

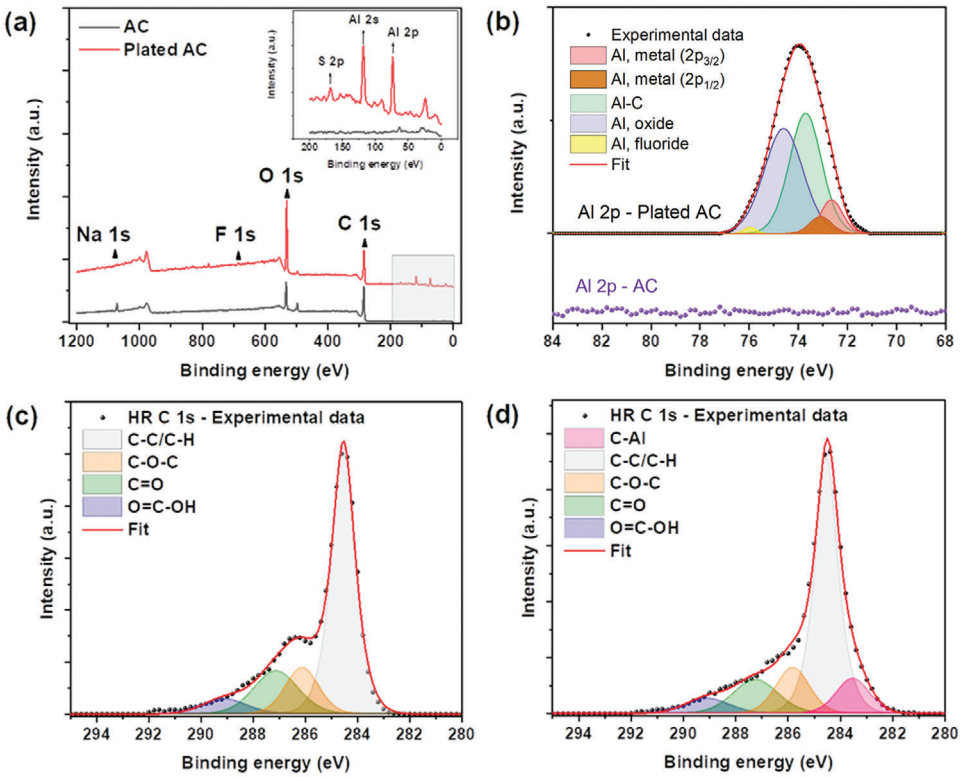

Figure 5. XPS results for bare AC sample and AC after the electrodeposition: a) survey spectra; b) Al 2p region; c,d) C 1s region.

area is reduced by 34.3 %. Interestingly, according to the t-plot micropore and external surface areas variations, most of the deposition seems to proceed preferably within micropores since the relative variations are 37.3 % and 25.5 %, respectively. Moreover, the micropore volume reduces of 38 % and the overall micro and meso porous volume reduces of 33 % implying that indeed, most of the deposition process is happening within micropores.

Finally, XPS measurements were carried out to unravel the nature of the deposited material, i.e., whether it was an electrochemically deposited layer or only an adsorbed one. The results are reported in **Figure 5**. Figure 5a shows the XPS survey scans collected for both analyzed samples while the semiquantitative analysis is shown in Table S1 (Supporting Information). Al 2s and Al 2p signals were successfully detected only in the case of the sample named *PlatedAC*, i.e., after the electrochemical deposition. No Al signal was detected from the bare sample. Additional information was obtained by collecting the high-resolution spectra for the Al 2p and C 1s regions. Figure 5b confirms that no Al was present in the bare sample while the Al 2p signal of sample *PlatedAC* could be fitted with several components. The first couple of peaks are positioned at ≈73 eV with a doublet splitting of 0.42 eV and represent the spin-orbit coupling doublets of Al in metallic state (Al $2p_{3/2}$ and Al $2p_{1/2}$).[35] The next one at increasing binding energy is at ≈73.4 eV and associated with Al-C bonds, confirming the formation of a stable interface between the electrodeposited Al coating and the underlying carbon-based support.[35,36] As described by Hinnen et al., the intensity of these peaks is influenced by the thickness of the deposited aluminum layer.[36] In our case, the ratio between the Al-C and Al-Al components is greater than one (see Table S2, Supporting Information). Moreover, the C 1s contribution coming from the underlying AC electrode (see Table S3, Supporting Information, and Figure 5) is still detectable and rather intense. Therefore, it can be inferred that the thickness of the deposited film is comparable with the XPS penetration depth (≈3–10 nm). The component centered at ≈74.4 eV is related to aluminum oxides/hydroxides.[37] It is worth mentioning that aluminum–oxygen compounds cannot be clearly distinguished by XPS as the corresponding binding energies highly overlap each other.[37] Finally, the last component in the high binding energy portion of the spectrum is due to fluoroaluminates residues from the decomposition of the electrolyte.[38,39] While the HR spectra of the Al component do not seem to be influenced by the decomposition products of the electrolyte after the thermal treatment, a significant change can be seen in the spectra of the fluorine component (see Figure S7, Supporting Information). In the case of the fluorine, indeed, while one can see the predominance of fluoroaluminate and organic fluorides in the sample treated at lower temperatures, instead after the heat treatment at 500 °C the major source of fluorine seems to be the metal fluoride component, which could be arising from a partial decomposition of the Na-CMC or from the impurities of the carbonaceous active materials.[38,40,41]

Figure 5c shows the C 1s region for the bare sample, which could be fitted with four separate components. The main one is associated with hydrocarbon/carbon in sp^2 hybridization state (284.5 eV, C–C sp^2/C–H) while the others are due to carbon-oxygen compounds: ether (C–O–C, 286.0 eV), carbonyl (C=O, 287.1 eV) and carboxyl (O=C–OH, 289.1 eV) functional groups.

Similar features are observed for the sample *Plated AC*, as shown in Figure 5d. However, an additional component in the low binding energy region (283.2 eV) is found, close to literature reports and associated with the presence of Al–C bonds.[36] These results are supporting the hypothesis of a thin Al film deposited on the AC with the proposed method, suggesting that two hours of deposition are not sufficient to get bulk Al deposited over the AC surface and that most likely the process proceeds uniformly in the active material volume.

3. Conclusions

The electrodeposition of aluminum on an amorphous carbon surface, stainless steel, and copper foil in an ACN based electrolyte was presented in this work. A thorough characterization of the deposition process results was carried out by means of elemental spectroscopies, morphological, and thermal characterizations. The present discovery opens the opportunities to deepen the process knowledge, allowing for a more efficient bath solution and opening the possibility to deposit a uniform aluminum phase without any chloro-aluminate salt. It is not excluded that this discovery could also open the possibility to the development of aluminum based electrochemical energy storage devices. The development of chloro-aluminate free electrolytes opens the possibilities to develop safer and cost-effective processes for aluminum plating, which is still a good technological solution to develop coatings against corrosion, to improve the wear resistance and aesthetic appeal of surfaces. However, deeper insights must be given into the deposition mechanism on the carbon surface to better exploit the observed phenomena, especially the different effects on carbon blacks and activated carbons.

4. Experimental Section

Electrolyte Preparation: Tetraethylammonium bis-trifluoromethylsulfonyl imide (Et_4N TFSI) was purchased by IoliTec, while aluminum bis-trifluoromethylsulfonyl imide (Al $TFSI_3$), solid at room temperature, was synthesized as reported in reference.[16] Acetonitrile (ACN) of anhydrous grade was purchased by Sigma Aldrich.

Solutions of 1 M TFSI anion were prepared to compare the effects of the different salts on the aluminum dissolution process. The experiments were carried out then at 1 N concentration meaning 1 M Et_4N TFSI in ACN and 0.33 M Al $(TFSI)_3$ in ACN.

Electrolytes were prepared under a controlled atmosphere environment in a MBrown Glove Box. The moisture and oxygen levels were below 0.1 ppm. Salts were weighted on an analytical balance. Electrolytes were prepared in a 5 mL flask.

Electrodes Preparation: Composite electrodes containing Activated Carbon (AC) YP-50F from Kuraray, Carbon Black (CB) C65 from Cabot, and Carboxyl Methylcellulose (CMC) from MTI were prepared. The slurry was prepared with DI water whose conductivity was 55 µS cm^{-1}. Powders were mixed according to the mass percent composition of 85% AC, 10% CB, and 5% CMC in a controlled amount of water that is 0.1 mL $mg_{CMC}{}^{-1}$. The slurry was prepared in a closed system to preserve the water content. CMC was added to heated water at 60 °C and dissolved while stirring with a cross-shaped magnetic stir bar. CB was added upon CMC complete dissolution, i.e. when a clear solution was obtained. AC was finally added when CB reached a homogeneous dispersion in the viscous media, then the heating was switched off. After 24 h stirring, the mixture got the aspect of a uniform ink, and it was coated over an aluminum current collector by means of a doctor blade procedure. The wet height of the coating was 150 µm and the coating speed was 30 mm s^{-1}. The final dry electrode mass loading was 2.0 mg cm^{-2}.

Counter electrodes for three electrodes measurements were fabricated according to the following procedure. AC DLC Super 30-company, CB C65, and PTFE (60 wt.% in water dispersion, purchased from Sigma–Aldrich). The materials were dispersed in a controlled amount of Ethanol (EtOH) equal to 20 mL $g_{tot}{}^{-1}$ according to the weight percentage of 85% AC, 10% CB, and 5% PTFE. The solution was stirred at a temperature set such that light bubbling could be observed by naked eye. The solution was left stirring until the slurry got the consistency of a dough. At this point, electrodes were directly punched out and baked at 100 °C.

Aluminum was pre-treated in a 5% KOH aqueous bath at 60 °C for 30 s to clean its surface. The aluminum foil was then rinsed with EtOH and DI water to clean the surfaces after the etching process.

Cell Assembling: Electrochemical cells were assembled in a controlled environment of an MBrown Glove Box with Argon atmosphere. Moisture and oxygen levels were below 0.1 ppm. Electrodes were piled in a Swagelok T-Cell made of stainless steel. All the electrodes were separated by means of Whatman Glass Fiber of grade D drenched with 120 µL of electrolyte. The separator between the electrode had a diameter of 12 mm, while the one used to separate the reference to the cell was 10 mm in diameter. To prevent short circuits, mylar foils were used to electrically isolate the cell chamber.

Physical–Chemical, Electrochemical, and Morphological Characterization: Electrolytes viscosities were measured by means of Anton Paar Rheometer MCR 102. The temperature range was [−30,80] °C with steps of 10 °C. Shear rate was set to 1000 s^{-1} at −30 °C, 2000 s^{-1} in the range [−20,−10] °C, 3000 s^{-1} at 0 °C and 4000 s^{-1} in the range [10,80] °C. The measurement at each temperature point was carried out for 30 s and viscosity was sampled every 3 s. The sample volume was 500 µL.

Electrolytes conductivities were measured by means of Modulab XM PSTAT (Solartron analytical-AMETEK, USA). Frequencies were swept from 300 kHz down to 1 Hz, with sinusoidal signals with 5 mV of peak amplitude. The ESR was evaluated to calculate the electrolyte conductivity according to the probe cell constant. The conductivity probe was made of parallel plates of black platinum and the sample volume was always 500 µL.

Electrochemical measurements were run with BioLogic VMP3. All the electrochemical experiments were starting with 1.5 h open circuit potential (OCP) or open circuit voltage (OCV) measurements according to the cell configuration, to let the electrochemical cells thermalize. Dissolution experiments were characterized by an LSV period starting from OCP up to 1.7 V versus Ag pseudo-ref with a scan rate of 1 mV s^{-1}. Then, the potential of 1.7 V was retained for 12 h at a constant voltage phase ("floating"). The current range was set as automatic, the voltage resolution was 100 µV and charges were measured over 100% of the voltage steps and averaged over 10 points so that the final voltage sampling was 1 mV. Electroplating measurements were performed in galvanostatic mode. Voltages were limited to a positive limit of 1.7 V versus Ag pseudo-ref for the anode, the working electrode, and −2 V versus Ag pseudo-ref for the cathode, the counter electrode. Sampling was set to 5 mV variation of the voltage between anode and cathode or every 10 s.

Charges were evaluated according to the following formula:

$$Q = \int i(t)\, dt \tag{1}$$

where Q is the electric charge in Coulombs, C, obtained via electric current, i, in Amperes, A, integration in time, expressed in second, s. To convert in Ah: $Q = Q[C]/3.6$.

The thermal analysis was carried out with a STA 6000 from Perkin Elmer. The gas flow was set to 20 mL N_2 per minute. The calibration of the equipment was carried out for nitrogen using indium, zinc, and silver and measuring the melting enthalpies. The oven temperature was ramped up from room temperature to 700 °C with 20 K min^{-1}. Fast Energy-dispersive X-Ray Spectroscopy (EDS) was performed by means of Phenom XL by acquiring samples at 15 keV in a mapping of 128×128 pixels images. Finer electron microscopy analyses were performed thanks to a field-emission scanning

electron microscope (FESEM Supra 40, Zeiss) equipped with a Si(Li) detector for energy-dispersive X-ray spectroscopy.

X-ray photoelectron spectroscopy (XPS) was carried out with a PHI 5000 VersaProbe (Physical Electronics) equipped with a monochromatic Al Kα radiation (1486.6 eV energy) as X-ray source. Different pass energy values were used for the survey (187.75 eV) and high-resolution (HR) spectra (23.5 eV) acquisition. Charge compensation during the measurements was accomplished with a combined electron and Ar^+ neutralizer system. HR spectra were analyzed after Shirley background subtraction, with CasaXPS software (version 2.3.18) and fitted with mixed Gaussian-Lorentzian components. Binding energy was calibrated with respect to C 1s position for adventitious carbon (284.5 eV).

Specific Surface Area (SSA) measurements were carried out on both bare and plated electrodes to investigate were the deposition takes place. N_2 adsorption isotherms were performed at 77 K by means of ASAP2020Plus, Micromeritics. The input weights for the SSA calculations were always the ones of the active materials masses. Samples analyzed after the electrodeposition processes were rinsed in acetonitrile prior to SSA measurements to remove as much as possible salt residuals.

Supporting Information

Supporting Information is available from the Wiley Online Library or from the author.

Acknowledgements

L.H.H. and A.B. wish to thank the Deutsche Forschungsgemeinschaft (DFG) for the financial support within the Projects "The combined use of computational screening and electrochemical characterization for the identification of new electrolyte components for supercapacitors" (BA 4956/5-1).The authors wish to thank Ms. Beate Fähndrich (Friedrich Schiller Universitat – Institute for Technical Chemistry and Environmental Chemistry and Centre for Energy and Environmental Chemistry Jena (CEEC Jena)) for the technical support.

Conflict of Interest

The authors declare no conflict of interest.

Data Availability Statement

The data that support the findings of this study are available on request from the corresponding author. The data are not publicly available due to privacy or ethical restrictions.

Keywords

activated carbons, aluminum dissolution, aluminum electroplating, electrodeposition, electroplating, supercapacitors

Received: February 14, 2023
Revised: May 2, 2023
Published online: June 4, 2023

[1] J. Rocabert, R. Capo-Misut, R. S. Munoz-Aguilar, J. I. Candela, P. Rodriguez, *IEEE Trans Ind Appl* **2019**, *55*, 1853.
[2] B. Babu, P. Simon, A. Balducci, *Adv. Energy Mater.* **2020**, *2001128*, 2001128.
[3] P. Kurzweil, M. Chwistek, *J. Power Sources* **2008**, *176*, 555.
[4] P. W. Ruch, D. Cericola, A. Foelske, R. Kötz, A. Wokaun, *Electrochim. Acta* **2010**, *55*, 2352.
[5] D. Cericola, R. Kötz, A. Wokaun, *J. Power Sources* **2011**, *196*, 3114.
[6] L. Köps, F. A. Kreth, A. Bothe, A. Balducci, **2022**, *44*, 66.
[7] C. Schütter, S. Pohlmann, A. Balducci, *Adv. Energy Mater.* **2019**, *9*, 1900334.
[8] S. Ozdemir, C. Varlikli, I. Oner, K. Ocakoglu, S. Icli, *Dye. Pigment.* **2010**, *86*, 206.
[9] J. Krummacher, L. H. Hess, A. Balducci, *J. Electrochem. Soc.* **2019**, *166*, A1763.
[10] Y. P. Yang, A. C. Huang, Y. Tang, Y. C. Liu, Z. H. Wu, H. L. Zhou, Z. P. Li, C. M. Shu, J. C. Jiang, Z. X. Xing, *Polymers* **2021**, *13*, 1675.
[11] J. Krummacher, L. H. Heß, A. Balducci, *ChemSusChem* **2017**, *10*, 4178.
[12] X. Wang, E. Yasukawa, S. Mori, *Electrochim. Acta* **2000**, *45*, 2677.
[13] E. Krämer, T. Schedlbauer, B. Hoffmann, L. Terborg, S. Nowak, H. J. Gores, S. Passerini, M. Winter, *J. Electrochem. Soc.* **2013**, *160*, A356.
[14] M. Morita, T. Shibata, N. Yoshimoto, M. Ishikawa, *Electrochim. Acta* **2002**, *47*, 2787.
[15] R. S. Kühnel, M. Lübke, M. Winter, S. Passerini, A. Balducci, *J. Power Sources* **2012**, *214*, 178.
[16] J. Krummacher, A. Balducci, *Chem. Mater.* **2018**, *30*, 4857.
[17] G. A. Elia, K. V. Kravchyk, M. V. Kovalenko, J. Chacón, A. Holland, R. G. A. Wills, *J. Power Sources* **2021**, *228870*, https://doi.org/10.1016/j.jpowsour.2020.228870.
[18] G. A. Elia, K. Marquardt, K. Hoeppner, S. Fantini, R. Lin, E. Knipping, W. Peters, J. F. Drillet, S. Passerini, R. Hahn, *Adv. Mater.* **2016**, *28*, 7564.
[19] A. M. Bittner, M. Zhu, Y. Yang, H. F. Waibel, M. Konuma, U. Starke, C. J. Weber, *J. Power Sources* **2012**, *203*, 262.
[20] D. B. Keyes, S. Swann, W. Klabunde, S. T. Schicktanz, *Ind Eng Chem* **1928**, *39*, 87.
[21] D. E. Couch, A. Brenner, **1951**, 234.
[22] Y. Zhao, T. J. VanderNoot, *Electrochim. Acta* **1997**, *42*, 3.
[23] R. Böttcher, A. Valitova, A. Ispas, A. Bund, *Trans. Inst. Met. Finish.* **2019**, *97*, 82.
[24] A. Despić, V. P. Parkhutik, **1989**, 401.
[25] K. Dejun, W. Jinchun, *J. Alloys Compd.* **2015**, *632*, 286.
[26] K. K. Maniam, S. Paul, *Coatings* **2021**, *11*, 80.
[27] Z. Slim, E. J. Menke, *J. Phys. Chem. C* **2022**, *126*, 2365.
[28] S. Pohlmann, R. S. Kühnel, T. A. Centeno, A. Balducci, *ChemElectroChem* **2014**, *1*, 1301.
[29] J. Krummacher, C. Schütter, S. Passerini, A. Balducci, *ChemElectroChem* **2017**, *4*, 353.
[30] X. Zhao, Y. Yin, Y. Hu, S. Y. Choe, *J. Power Sources* **2019**, *418*, 61.
[31] W. Liu, P. Liu, D. Mitlin, *Adv. Energy Mater.* **2020**, *10*, 2070177.
[32] F. Jiang, S. Yang, H. Liu, X. Cheng, L. Liu, R. Xiang, Q. Zhang, S. Kaskel, J. Huang, *SusMat* **2021**, *1*, 506.
[33] G. Guvendikand, D. R. Gabe, *Trans. Inst. Met. Finish.* **1999**, *77*, 127.
[34] J. Sun, S. L. Simon, *Thermochim. Acta* **2007**, *463*, 32.
[35] C. D. Wagner, A. V. Naumkin, A. Kraut-Vass, J. W. Allison, C. J. Powell, J. R. J. Rumble, **2012**, https://doi.org/10.18434/T4T88K.
[36] C. Hinnen, D. Imbert, J. M. Siffre, P. Marcus, *Appl. Surf. Sci.* **1994**, *78*, 219.
[37] P. M. A. Sherwood, *Surf. Sci. Spectra* **2002**, *9*, 62.
[38] A. Hess, E. Kemnitz, A. Lippitz, W. E. S. Unger, D. H. Menz, *J. Catal.* **1994**, *148*, 270.
[39] J. Y. Lin, Y. L. Chen, X. Y. Hong, C. Huang, C. P. Huang, *J. Colloid Interface Sci.* **2020**, *561*, 275.
[40] H. Cai, G. Chen, C. Peng, L. Xu, Z. Zhang, F. Ke, X. Wan, *RSC Adv.* **2015**, *5*, 101819.
[41] G. Beamson, D. Briggs, **1992**, *76*, 919.